

RESEARCH

Open Access



Stressing State Analysis of Reinforcement Concrete Beams Strengthened with Carbon Fiber Reinforced Plastic

Jie Huang^{1,3}, Jun Shi^{1,2*} , Hengheng Xiao³, Jiyang Shen³ and Baisong Yang³

Abstract

This paper investigated the working behavior characteristics of six reinforcement concrete (RC) beams subjected to bending based on the numerical shape function (NSF) method and structural stressing state theory. Firstly, the structural stressing state mode is expressed based on the generalized strain energy density (GSED) derived from the measured strain data. Then, one of the Carbon Fiber Reinforced Plastic (CFRP)-strengthened RC beams is taken as an example and the leap characteristics of RC beam's stressing state are detected by applying the Mann–Kendall (M–K) criterion, updating the existing definition of the structural failure load. Accordingly, the stressing state modes and strain fields of the CFRP-strengthened RC beam are proposed to reveal their leap characteristics. Furthermore, through comparing the working performance of six RC beams, the effects of different strengths and different reinforcement ratios on CFRP strengthening performance are investigated. Finally, the NSF method is applied to reasonably interpolate the limited strain data for further revealing the stressing state characteristics of the RC beams. The research results explore a new analysis method to conduct an accurate estimation of the structural failure load and provide a reference for the future design of CFRP-strengthened RC beams.

Keywords: stressing state, leap, failure load, stressing state mode, numerical shape function, CFRP, reinforcement concrete beam

1 Introduction

Reinforced concrete (RC) structures are extensively used in civil engineering construction and most of the existing RC structures are in need of reinforcement and maintenance due to corrosion, freezing and thawing cycle, sulfate attack, and physical damage from impacts. (Toutanji et al. 2006; Benjeddou et al. 2007; Rafi et al. 2008; Hawileh et al. 2015). To tackle this problem, Fiber Reinforced Plastic (FRP) has been widely adopted in strengthening

and retrofit of structural members, such as slabs, beams, and columns (Bousahla et al. 2020; Medani et al. 2019; Draoui et al. 2019; Karami et al. 2019). The FRP materials are known to have the high strength-to-weight ratio, high durability, electromagnetic neutrality, ease of installation, resistance to corrosion, rapid execution with low labor, and practically unlimited availability in size, geometry and dimension of these materials (Ali et al. 2014; Salama et al. 2019; Hawileh et al. 2014). Carbon Fiber Reinforced Polymer (CFRP) possibly enhances the mechanical properties of concrete compared to other types of FRP owing to its larger modulus and tensile strength. Therefore, the strengthening technique of using CFRP is extensively and rapidly increasing in the construction field (Abualnour

*Correspondence: hitshijun@hit.edu.cn

² National Engineering Laboratory for High Speed Railway Construction, Changsha, China

Full list of author information is available at the end of the article

Journal information: ISSN 1976-0485 / eISSN 2234-1315

et al. 2019; Draiche et al. 2019; Belbachir et al. 2019; Sahla et al. 2019).

In order to investigate the behavior of strengthened structures or members by CFRP, various experiments of this innovative strengthening method have been conducted after the 21th century. Experimental studies have demonstrated (Hawileh et al. 2015; El-Ghandour 2011; Attari et al. 2012; Balamuralikrishnan and Jeyasehar 2009) that externally bonded CFRP can be used to effectively improve the desired performance of a structural member such as its load carrying capacity, flexural strength, stiffness, ductility, durability, as well as performance under cyclic and fatigue loading. Spadea et al. (2001) investigated the strength and ductility aspects of RC beams strengthened with an externally bonded CFRP laminate and found that the significant increases in strength obtained by strengthening with bonded CFRP laminates are at the expense of ductility. Li et al. (2006) performed an experimental study to predict the loading carrying capacity of RC beams strengthened with CFRP composites. The results of tests verified that, in contrast with a control beam, initial cracking loads of strengthened beams increase slightly, whilst stiffness and ductility increase more and the ultimate loads increase considerably. Altin et al. (2010) manufactured 10 T cross-sectioned half-scale simply supported beam specimens to obtain ductile flexural behavior for shear-deficient RC beams and found that CFRP strips without anchorages improved the shear strength of shear deficient beams, but they cannot prevent the shear failure. Besides, Dias et al. (2018) carried out an experimental program to investigate the flexural behavior of RC beams strengthened using the NSM technique with CFRP laminates. The experimental results show that NSM CFRP laminates is an effective solution to increase flexural strength, cracking, yielding and maximum loads of beams failing in bending.

In addition, extensive studies were conducted to identify the experimental parameters (the length, thickness, position, form and layer number of CFRP, the shear span ratio, reinforcement ratio and concrete strength of the experimental beam, etc.) effect on the structural behavior of RC beams strengthened with CFRP. Ashour et al. (2004) studied the effect of different parameters including the length, thickness, position and form of the CFRP on the failure of 16 RC beams with external CFRP laminates. The findings verified that when the two-layer fibers are used for strengthening, the increase of the length of the second layer of the fiber on the performance of beams approaches a constant value if the length of the second layer reaches some limit. Osman et al. (2019) undertook experimental and numerical studies to investigate the performance of seven RC beams under four-point loading with different concrete

strength, shear span-to-depth ratios, longitudinal and vertical reinforcement ratios. The results found that as the longitudinal reinforcement ratio is increased, there is a small increase in the concrete shear strength, and the contribution of CFRP laminates on the load capacity and rigidity of repaired RC beams is significant for any concrete strength class.

From the literature above, the lack of sufficient experiments on RC beams strengthened with CFRP to investigate the effect of beam parameters on the performance of RC beams can be seen. Besides, the above literature focused on single aspects of failure, such as reinforcement ratio or concrete strength. To some extent, the high test cost limits the development of research on CFRP-strengthened RC beams. Furthermore, the measured strain data has always been underutilized in existing experimental analysis, leading to the neglect of valuable unseen information about structural working behavior characteristics. Therefore, it is significant to apply an innovative and appropriate method to analyze the working behavior of CFRP-strengthened RC beams on the basis of existing experimental data. In addition, the finite element simulation of CFRP-strengthened RC beams inevitably adopts experiential simplification, assumption, etc. Consequently, the simulation results of structural responses usually different from that of the actual experiment in different degrees, which makes it difficult to reflect the structural change characteristics through simulation.

In consideration of all these problems, this paper applies the innovative methods to reveal the undiscovered the stressing state characteristics of CFRP-strengthened RC beams under loading processes. According to the structural stressing state theory, the strains of all measuring points of the CFRP-strengthened RC beam are modeled as generalized strain energy density (GSED) to describe the RC beams' stressing state modes and the sum of GSED is introduced as a characteristic parameter to express the RC beams' stressing state. Then, the Mann–Kendall (M–K) criterion is used to distinguish the characteristic loads. Additionally, the effects of different concrete strengths and reinforcement ratios on the RC beams' performance can be revealed by comparing the stressing state modes of RC beams established by the measured strain data. Finally, Using the numerical shape function (NSF) method to interpolate the limited experimental data, the strain fields and internal forces of the RC beams are obtained to further analyze the structural behavior. The results achieved in this paper could provide a reference for the research and design improvement of RC beams and other structures strengthened by CFRP in the future.

2 Method and Theories of Structural Stressing State

2.1 Structural Stressing State Concept

The structural stressing state is the inner or outer modes of the structure (including the components/units or their combinations) under a certain loading case defined by Zhou et al. (2006), which can be characterized by the matrix or the vector consisting of structural responses, such as strains, deflection, GSEDs, internal forces, strain fields and so on. The structural stressing state is generally for the whole structure and component stressing state for individual structural components, local parts, and internal forces. The structural stressing state will change with the increase of load and manifest different characteristics at some special load levels, which complying the natural law from quantitative change to qualitative change of a system (Shi et al. 2018). Therefore, when the load reaches a certain value, the structural stressing state will inevitably present a qualitative mutation (shape change or amplitude change of stressing state mode). Here, this paper defines the load corresponding to the qualitative mutation of the structural stressing state as updated failure load, that is, the starting point of structural failure, so as to updating the existing analytical theories and analytical methods as well as the more reasonable design codes.

2.2 Modeling of Structural Stressing State

As mentioned above, the stressing state mode of the CFRP-strengthened RC beam is the numerical description of the working behavior characterized by structural responses. In order to construct the numerical mode expressed in the form of vector or matrix and the corresponding characteristic parameters, generalized strain energy density (GSED) is adopted to numerically describe the stressing state of a measured point (Huang et al. 2014). Therefore, for one measured point of the RC beam, its GSED value can be expressed as

$$E_{ij} = \int \sigma_1 d\varepsilon_1 + \sigma_2 d\varepsilon_2 + \sigma_3 d\varepsilon_3 \tag{1}$$

where E_{ij} is the GSED value of the i -th measuring point under the j -th load; $\sigma_1, \sigma_2, \sigma_3$ and $\varepsilon_1, \varepsilon_2, \varepsilon_3$ are three principal stresses and strains, respectively. Hence, in order to calculate the stressing state of the entire structure or some segments of the whole, GSED values of all concerned points should be summed, that is

$$E_j = \sum_{i=1}^n E_{ij} \tag{2}$$

where E_j is the structural GSED sum of all the measuring points under the j -th load, n is the total number of

points. Then, the $E-F_j$ curve can be plotted to investigate the structural stressing state features.

2.3 Mann–Kendall Criterion

The Mann–Kendall (M–K) method as a nonparametric statistical method is generally used in trend analysis without the necessity for samples to conform with certain distributions or interference of a few outliers, and the leap characteristics of the structure can be detected from the $E-F$ curve (Mann 1945; Kendall 1948; Hirsch et al. 1982). It is assumed that the sequence of $\{E_j(i)\}$ (the i -th load step, i is 1, 2, ..., n) is statistically independent, and a new stochastic variable Q_k at the k -th load step is defined as

$$Q_k = \sum_i^k D_i \quad (2 \leq k < n) \tag{3}$$

$$D_i = \begin{cases} +1 & E_i > E_j (1 \leq j \leq i) \\ 0 & \text{otherwise} \end{cases} \tag{4}$$

where h_i is the cumulative number of the samples; “+1” means adding one more to the existing value if the inequality on the right side is satisfied for the j th comparison. The mean value $E(Q_k)$ and variance $V(Q_k)$ are calculated by

$$E(Q_k) = \frac{k(k-1)}{4} \quad (2 \leq k \leq n) \tag{5}$$

$$V(Q_k) = \frac{k(k-1)(2k+5)}{72} \quad (2 \leq k \leq n) \tag{6}$$

Then, a new statistic UF_k is defined by

$$UF_k = \begin{cases} 0 & k = 1 \\ \frac{Q_k - E(Q_k)}{\sqrt{V(Q_k)}} & 2 \leq k \leq n \end{cases} \tag{7}$$

Accordingly, the UF_k-F_j curve can be plotted. The proceeding of the inverse $\{E_j(i)\}$ sequence is consistent with before, which can form the UP_k-F_j curve. Consequently, the intersecting point of the UF_k and UP_k curves is the characteristic load of the $E-F_j$ curve.

2.4 Method of Numerical Shape Function

In the structure analysis, to some extent, the limited data of structural responses collected from experiments can reflect the working behavior characteristics of the structure under loading. However, it cannot provide a full expression of the structural response mechanism and characteristics. Therefore, the method of numerical shape function (NSF) interpolation is proposed to obtain

detailed information about structural response through interpolating/expanding experimental data, which has clear physical significance. The NSF method is a new and effective interpolation method, which applies generalized numerical simulation of a specific ideal physical model to construct discrete weighting function based on the concept of shape function in the finite element method (FEM) (Ayers 2006; Padhi et al. 2001).

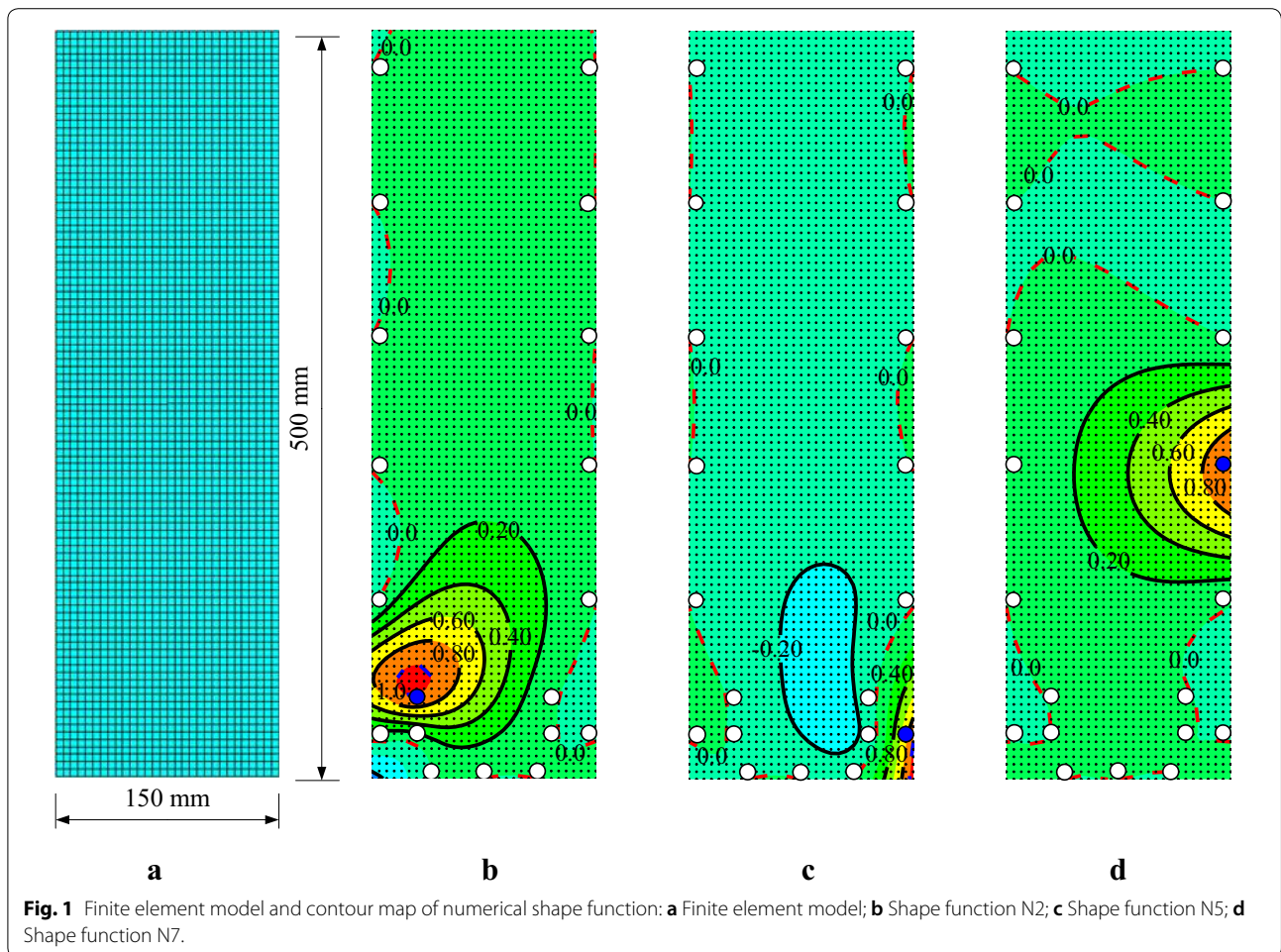
Here, in order to introduce this method, the deflection field of B3's mid-span section is used as an example. It can be seen from Fig. 1a that the section is constructed and properly meshed with element Shell 181 by ANSYS, and 19 measuring points are adopted as the sampled points of the NSF. Then, a unit displacement at measuring point *i* along the z-axis is applied to the section, while the other ones are fixed to restrict rigid displacements. Therefore, the numerical shape function N_i of the *i*th measuring point can be derived from FEM. As a result, Fig. 1a, b and c shows the shape function of N_2 , N_5 and N_7 , respectively. Without considering large deformation or elastoplasticity, the displacement field constructed by

Castigliano's theorem is independent of loading paths, and the linear superposition can be used for the simulative results that have explicit physical meanings. Hence, according to the deflection of the 19 sampled points, the deflection field is obtained by Eq. (8),

$$D = \sum_{i=1}^m u_i N_i, \quad N_i = [N_i(x_1), N_i(x_2) \cdots N_i(x_j) \cdots N_i(x_n)] \tag{8}$$

where D is the deflection field of the whole section, N_i is the numerical shape functions of *i*-th measuring point, $N_i(x_j)$ is the function value at element node x_j , n is the total number of element nodes, and $m=19$ is the total number of measured points.

Consequently, the limited experimental measuring strain on the cross-section could be expanded by the NSF interpolation to achieve strain fields and the internal forces distribution of the structure. Hence, this method could meet the requirements for in-depth experimental analysis and reveal global/local working characteristics of the structure.



2.5 Accuracy Verification of Expanded Experimental Data

In order to evaluate the accuracy of the NSF method, the measured strain at 17 points of the B3 beam's mid-span section are used to construct the strain filed, and then the interpolation results at the other two points (points 1 and 7) of the cross-section could be obtained. Therefore, these interpolation values are compared with the experimentally measured ones, and the error of the i -th point under the j -th load between them can be calculated by

$$\delta_{ij} = \left| \frac{\varepsilon_{ij}^s - \varepsilon_{ij}^e}{\varepsilon_{ij}^e} \times 100\% \right| \quad (9)$$

where δ_{ij} is the error of the i -th point under the j -th load between interpolation and experimental results, ε_{ij}^s and

ε_{ij}^e are respectively the interpolating and experimental strains of the i th point under the j -th load.

The average error of the i -th point during the whole loading process can be calculated by

$$\bar{\delta}_i = \frac{1}{N} \sum_j \delta_{ij} \quad (10)$$

where $\bar{\delta}_i$ is the average error of the i th point, N is the total number of load steps. Therefore, the accuracy of the NSF method could be demonstrated through the error values and the comparison curves between interpolation and experimental data.

Here, the measured points 1 and 7 are used as an example and the interpolation and experimental curves of them are plotted in Fig. 2 to reflect the accuracy of interpolation. The two curves for the same point have great fitting degrees even overlapping with each other in the whole loading process. The maximum and average errors of points 1 and 7 are respectively 11% and 6%, 11.7% and 7%. In addition, the interpolation results of other RC beams also present a great fitting degree, which could meet the requirement of the application. Hence, the NSF method could expand experimental data accurately so as to further investigate the structural working behavior of RC beams.

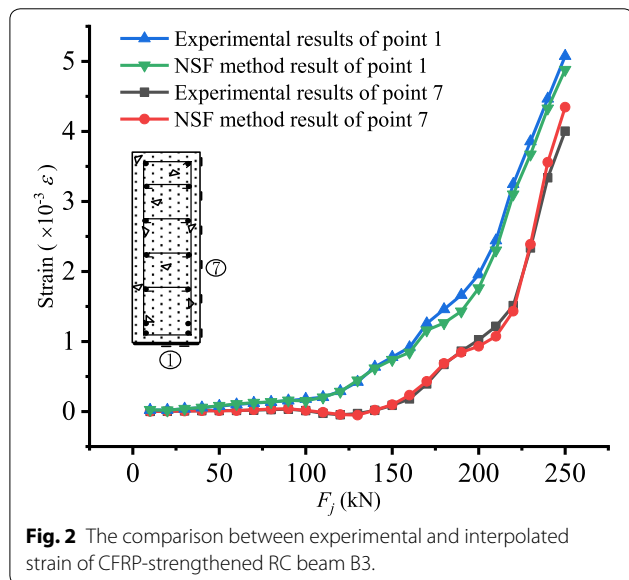


Fig. 2 The comparison between experimental and interpolated strain of CFRP-strengthened RC beam B3.

3 Experiment of RC Beams

3.1 Configuration of the RC Beams

He conducted the experiment of six RC beams with the same section labeled B1, B2, B3, B4, B5 and B6 (He 2016). As shown in Fig. 3, the experimental RC beam is 2300 mm in length, 4:1 in shear span ratio, 150 mm in width and 500 mm in height. In addition, the effective length is 2000 mm with two ends simply supported.

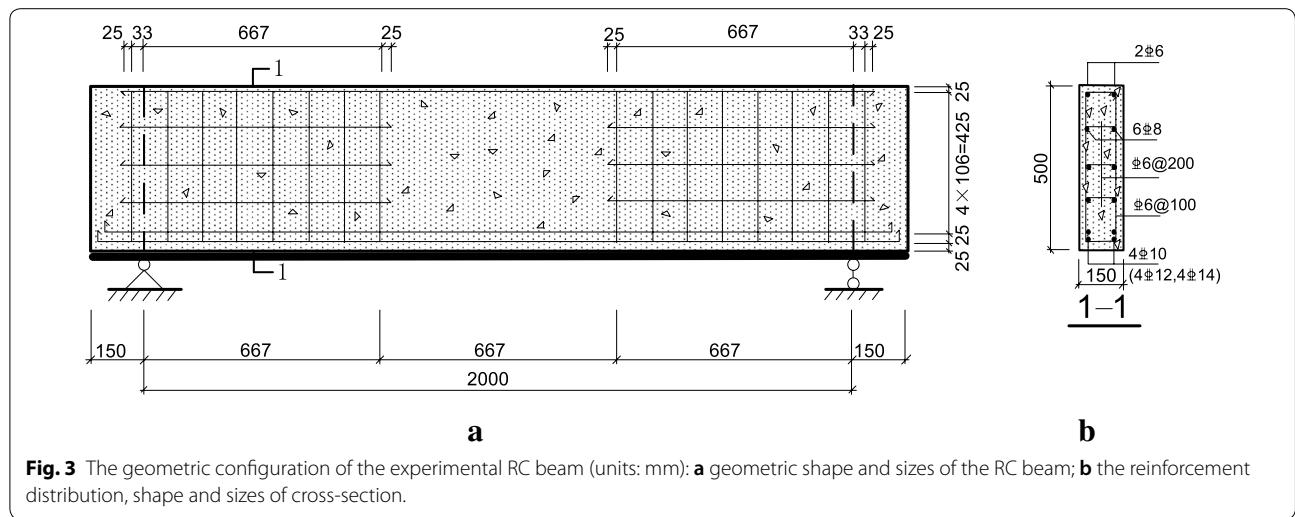


Fig. 3 The geometric configuration of the experimental RC beam (units: mm): **a** geometric shape and sizes of the RC beam; **b** the reinforcement distribution, shape and sizes of cross-section.

Figure 3b shows the section dimension and the configuration of the reinforcement. The tensile strength and elastic modulus of the CFRP sheet are 3512 MPa and 246 GPa. And the thickness of the single-layer CFRP sheet is 0.167 mm. Table 1 lists the detailed parameters of these experimental CFRP-strengthened RC beams.

3.2 Measuring Point Arrangement

Strains of two layers of longitudinal reinforcement and CFRP are recorded at the mid-span and 5L/12 cross-section and strains of concrete are recorded at the mid-span cross-sections. In addition, the concrete strain gauges are evenly distributed along the side of the beam at a distance of 90 mm. Figure 4a shows the arrangement of measuring points for the entire section of the RC beam. Figure 4b, c show the strain gauge arrangement of CFRP and reinforcements respectively.

3.3 Loading Scheme

As shown in Fig. 5, the concentrated load (F_0) is applied by jack at the mid-span of the experimental RC beam, then F_0 is allocated at three diving points through distributing beam. By employing step loading, F_0 increased 10 kN at each load level before cracking load, and after

cracking load F_0 increased 5 kN at each load level until the RC beam reaches the limit state.

4 Stressing State Analysis of the RC Beam B3

4.1 GSED-Based Structural Stressing State and Corresponding Characteristic Parameter

The GSED values of all measuring points on the mid-span cross-section are used to form a vector to represent the stressing state mode of RC beam, $S_j = [e_{M1}, e_{M2}, \dots, e_{Mi}, \dots, e_{MN}]^T$, in which e_i is the GSED value of the i point among N measuring points at the mid-span cross-section of RC beam. The corresponding characteristic parameter of S_j proposed to reveal the RC beam's stressing state features is expressed as the sum of the GSED values:

$$E_j = \sum_{i=1}^N e_{ij} \tag{11}$$

where e_{ij} is the GSED value of the i -th measuring point to the j -th load level; N is the number of measuring points of the mid-span section. Therefore, based on the GSED values, the structural stressing state is modeling by S_j and the corresponding characteristic parameter E_j at each load level is proposed to characterize the change of structural performance. Then, the $E-F_j$ curve can be utilized to investigate the leap features of RC beam's stressing state.

4.2 Investigation into the E-F_j Curve

Here, the sum of GSED values (E) under each load can be calculated by Eq. (2), then the $E-F_j$ curve can be plotted to reflect the changing characteristics of the structural stressing state. And two characteristic points P (100 kN) and Q (200 kN) in the $E-F_j$ curve are distinguished using the M-K criterion, as shown in Fig. 6. Accordingly, the structural stressing state during the

Table 1 The detailed parameters of experimental CFRP-strengthened RC beams.

Specimen number	Layer number	Concrete strength	Bottom reinforcement configuration
B1	0	C30	4C10
B2	1	C20	4C10
B3	1	C30	4C10
B4	1	C30	4C12
B5	1	C30	4C14
B6	1	C40	4C10

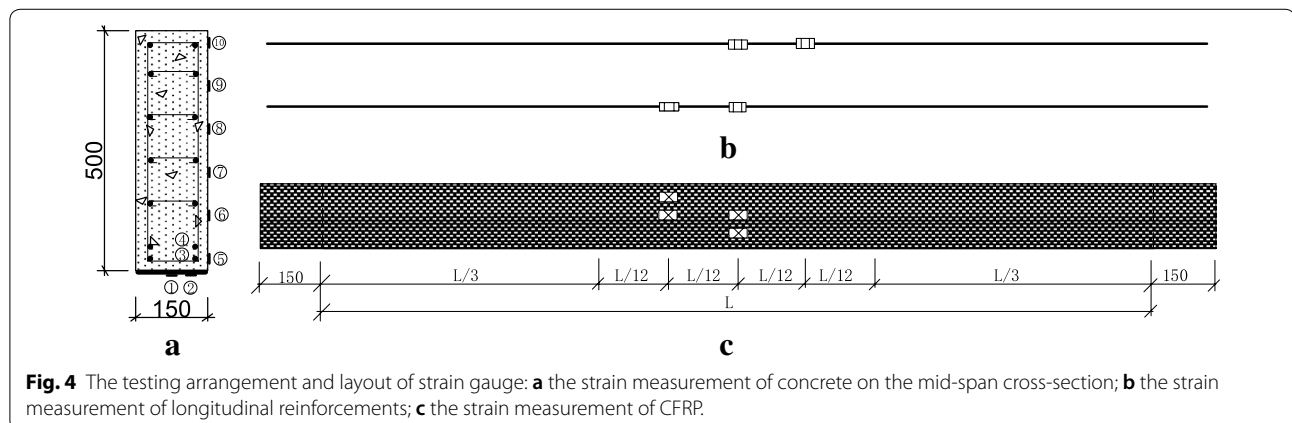


Fig. 4 The testing arrangement and layout of strain gauge: **a** the strain measurement of concrete on the mid-span cross-section; **b** the strain measurement of longitudinal reinforcements; **c** the strain measurement of CFRP.

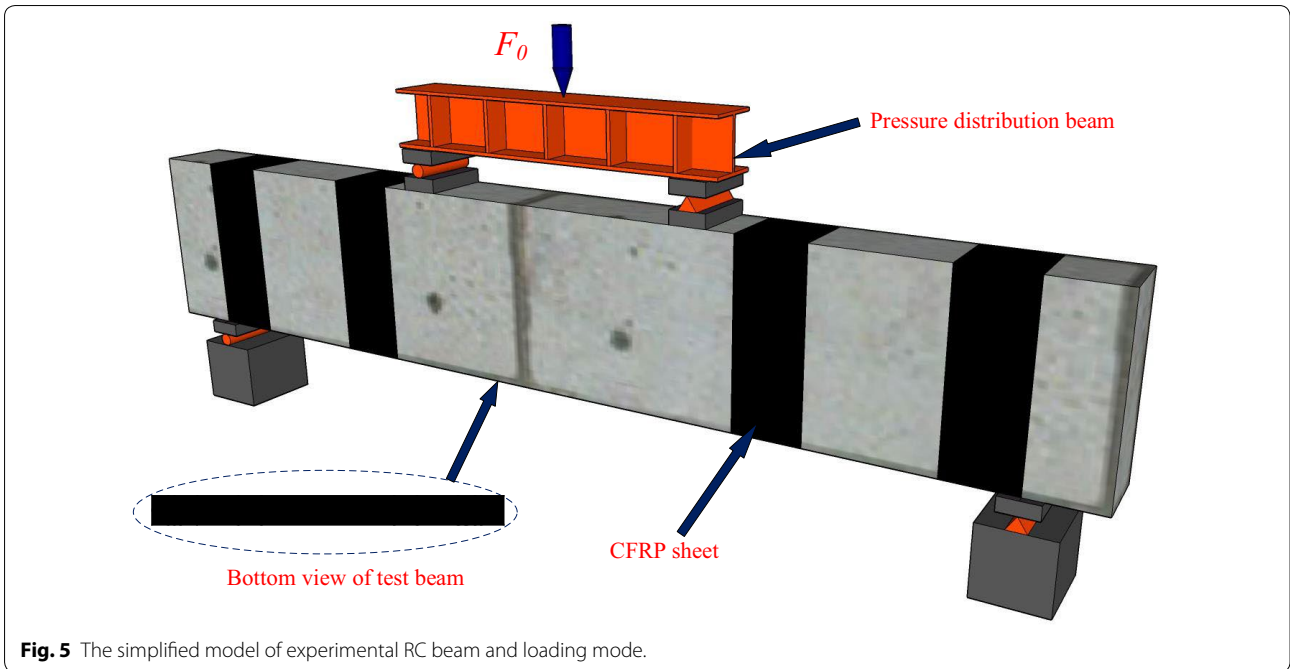


Fig. 5 The simplified model of experimental RC beam and loading mode.

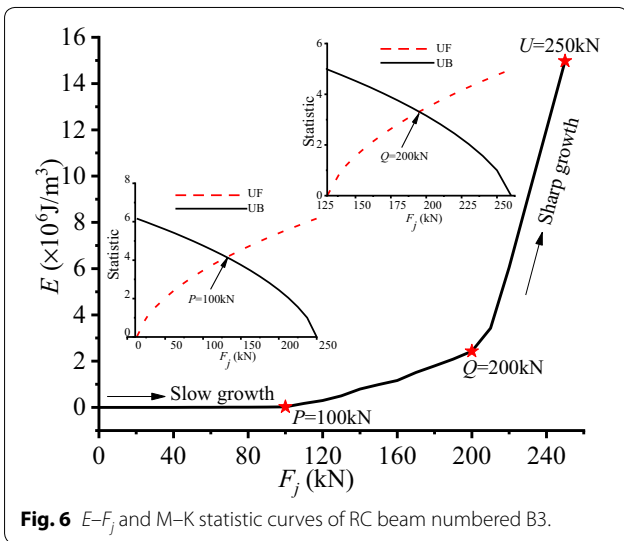


Fig. 6 $E-F_j$ and M-K statistic curves of RC beam numbered B3.

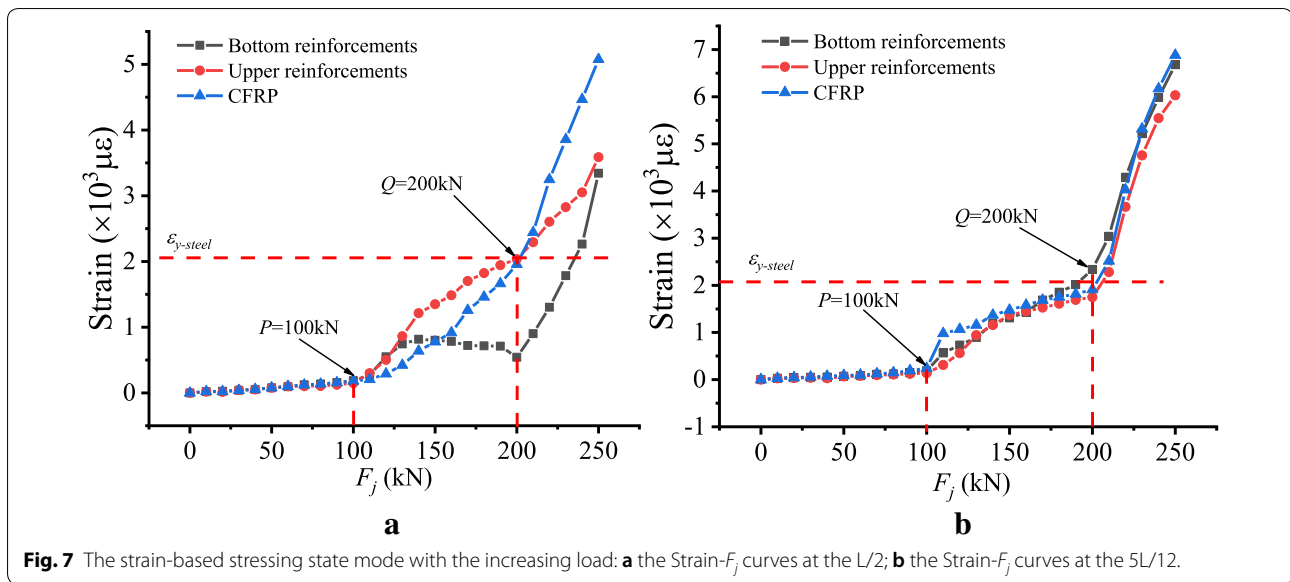
whole loading process can be divided into three stages by the two characteristic loads: (1) before the load P , the $E-F_j$ curve is basically in the stage of linear slow growth, signifying that the B3 RC beam is basically in quite stable linear-elastic stressing state. (2) from P to Q , the curve increases still slowly and steadily, but it shows nonlinear growth, which could be indicated that the B3 RC beam enters stable elastic-plastic stressing state due to the development of concrete crack. (3) After the load Q , the curve increases sharply probably due to the further plastic development of the B3 RC

beam, implying that the beam turns into an unstable stressing state from the stable stressing state.

Therefore, the characteristic load P can be seen as the demarcation point from an elastic working state to a plastic working state. Although a part of the concrete or reinforcement has been in the plastic working state, the sum of GSED value E of the beam is still in a relatively stable growth state. Thus, the tested RC beam still has stable performance. After the characteristic load Q , it is apparent that the stressing state of the tested RC beam appears mutation due to the continuous accumulation of plastic deformation, according with the natural law from quantitative change to qualitative change of a system. Therefore, the characteristic load Q is defined as the failure load, which could be seen as the termination of the previous stable stressing state. Moreover, it could also be regarded as the beginning of the structural failure process. Accordingly, load Q is defined as the failure load of the RC beam, which is updated the existing failure load (ultimate load) and reflects inherent mutation characteristic of the structural stressing state. That is to say, the mutation load of the structural stressing state is determinate and could be taken as the reference to the determination of structural design load.

4.3 Analysis of Structural Stressing State Mode Based on the Measured Strain

The trend changing curves of strain-based stressing state modes are plotted in Fig. 7a, b to detect the changing features of stressing state mode. It can be seen from



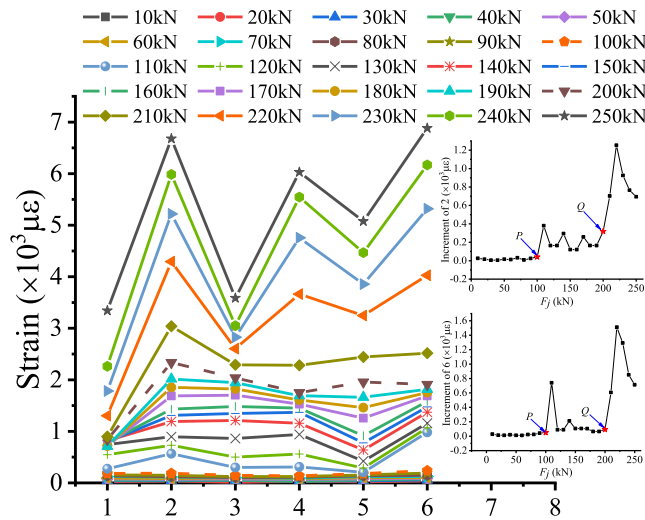
the Fig. 7 that the curves are divided into three different developing trends. Before the load P , the Strain- F_j curves almost keep linear growth, and bottom reinforcements, upper reinforcements and CFRP are in elastic stage without yield, indicating that the stressing state of B3 RC beam stays in a stable elastic stressing state. After that, the curves increase slowly and begin to separate, reflecting that B3 RC beam turns from linear-elastic state to elastic-plastic state. More specifically, From P to Q , the strain increases faster than the previous stage with the change of structural stressing state caused by the plastic deformation of sections. In addition, it is evident from Fig. 7a that the bottom reinforcements and upper reinforcements of section A are basically the same in the early stage of elastic-plastic state, but all the curves separate as the load increases. As shown in Fig. 7b, the development trend of bottom reinforcements, upper reinforcements and CFRP in elastic-plastic stage is basically the same. After load Q , all the curves mutate and the strain further increases rapidly with the load, manifesting that B3 RC beam begins to enter the unstable stressing state. It can be found in Fig. 7a that the strain of bottom reinforcements increases sharply and gradually reaches the yield strain caused by the yielding of upper reinforcements. Therefore, the stressing state modes reveal the leap characteristic at load P and load Q consisted with that distinguished by the M-K method in Fig. 6.

Meanwhile, the strain-based stressing state modes can be expressed through the other form as well. As shown in Fig. 8, the mutations of structural performance can also be confirmed, which is consistent with the law revealed in Fig. 8. More specifically, after the load Q (dashed lines), the strains increase sharply than previous stage, implying

the structural stressing state mode occurs mutation at failure load determined by the M-K criterion. Therefore, the increment of strain values with the increasing load can also reveal the leap features at the characteristic load Q . In addition, the increment of strain values can be regarded as the corresponding characteristic parameter of the strain-based stressing state mode.

4.4 Characteristic of Stressing State Mode for Plane-Section

Here, in order to investigate the changing process of RC beam's sectional working features, the strains of concrete along the height of mid-span cross section are constructed the sectional stressing state mode, $S_j = [s_{1j}, s_{2j}, s_{3j}, s_{4j}, s_{5j}, s_{6j}]^T$, in which j is load step and the s_{1j} , s_{2j} , s_{3j} , s_{4j} , s_{5j} and s_{6j} are the strains of measuring points under the j -th load. It is evident from Fig. 9 that the strain growth rate of the lower section is much faster than that of the upper section. As Fig. 9 shows, before 100 kN, the strain values of these six measuring points are basically in a straight line and all of them do not reach the $\epsilon_y = 330 \mu\epsilon$ (the cracking strain of concrete), manifesting that the mid-span cross section of RC beam maintains flat state during this load-bearing stage. After 100 kN, the concrete strains at the bottom of RC beam increase sharply on account of the intensive development of concrete crack. It can be seen from the Fig. 9 that the flat state of the section begins to embody a slight non-linear state caused by the elastic-plastic deformation of the RC beam but still keeps the basic flat state. Then, the flat state change of the mid-span cross section emerges at load Q , indicating that the plastic deformation will gradually develop to other locations. After the load Q ,



Note: 1 and 2 represent the bottom reinforcement at the L/2 and 5L/12, respectively. 3 and 4 represent the upper reinforcement at the L/2 and 5L/12, respectively. 5 and 6 represent the CFRP at the L/2 and 5L/12, respectively.

Fig. 8 The changing features of strain-based stressing state mode.

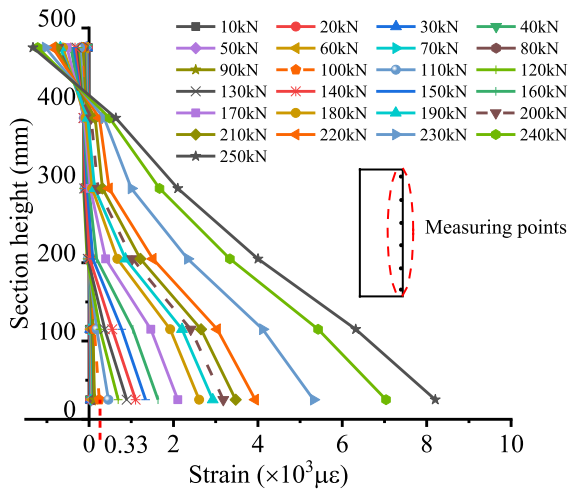


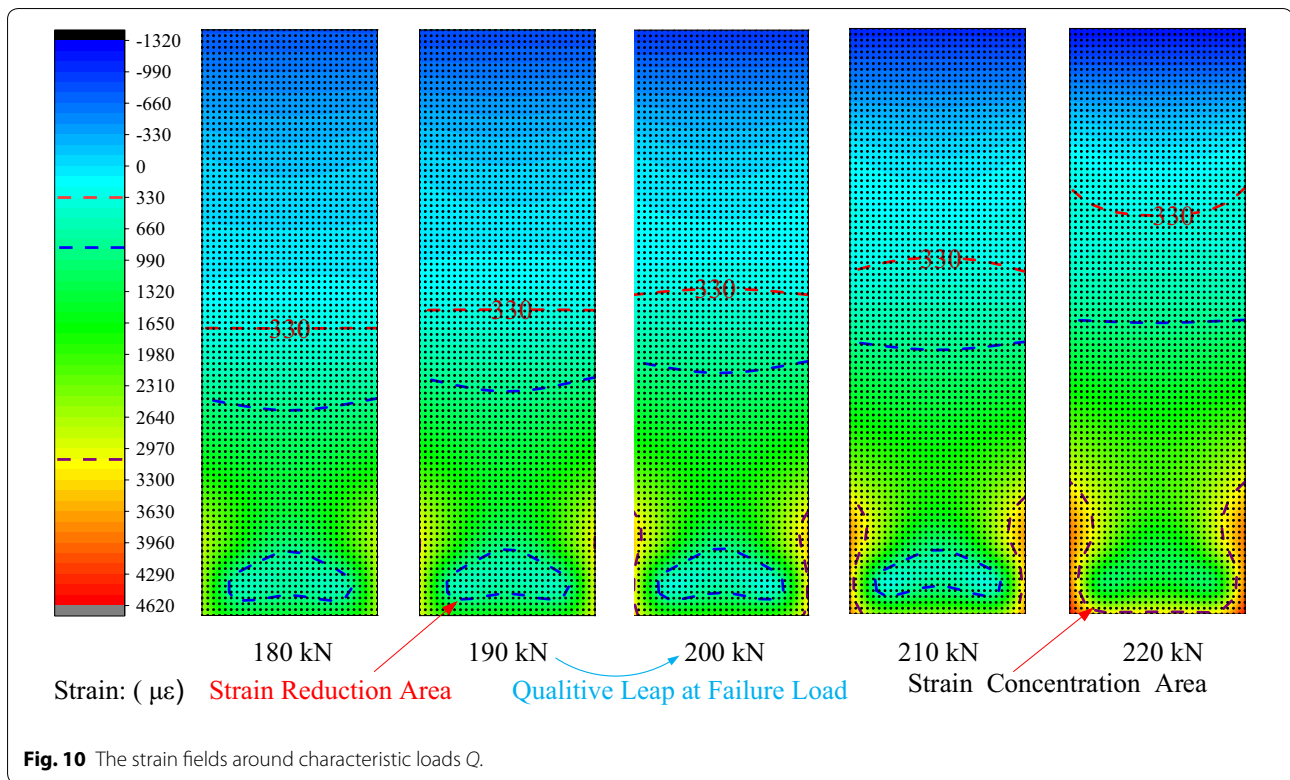
Fig. 9 Location-strain curves of mid-span cross section.

the concrete strains at the bottom of RC beam increased very sharply, signifying that the stressing state mode of the RC beam begins to change from the elastic-plastic state into plastic state and the concrete almost loses its bearing capacity due to the sufficient development of concrete cracks. The structural stressing state of RC beam changes from stable to unstable. Therefore, it is reasonable to define the load Q as the failure load of the RC beam, revealing the leap characteristic of the stressing state mode.

4.5 Change Characteristics Reflected by Strain Fields

Certainly, the performance features of RC beams around the updated failure load Q and their respective working behavior characteristics under loading can be reflected on the basics of experimental strain data in some extent. However, these limited data could only reflect the distribution and the development of strains of each measured point, that is, the local structural working features. Therefore, the NSF method is applied to the mid-span section of B3 RC beam, so as to obtain the strains at unmeasured points of the cross section. The change characteristics of the B3 RC beam’s structural stressing state can be described more intuitively by constructing the strain fields of the cross section. It is apparent from Fig. 6 that three stressing state stages of the B3 RC beam are divided by the two characteristic loads, respectively, the elastic, and failure one. Therefore, the strain fields of B3 RC beam around the characteristic load Q are plotted to investigate the changing characteristics of the cross section. Additionally, in the contour maps with the same color scale, the separatrix of 330 με (ultimate tensile strain), 880 με and 3080 με are marked with red, blue and brown dotted lines respectively to intuitively observe the distribution characteristics of strain area.

As depicted in Fig. 10, it can be seen that the region beyond ultimate tensile strain expands largely before and after 200 kN, indicating a qualitative leap at failure load Q. Besides, after the failure load 200 kN, the area of strain concentration expands continuously and rapidly.

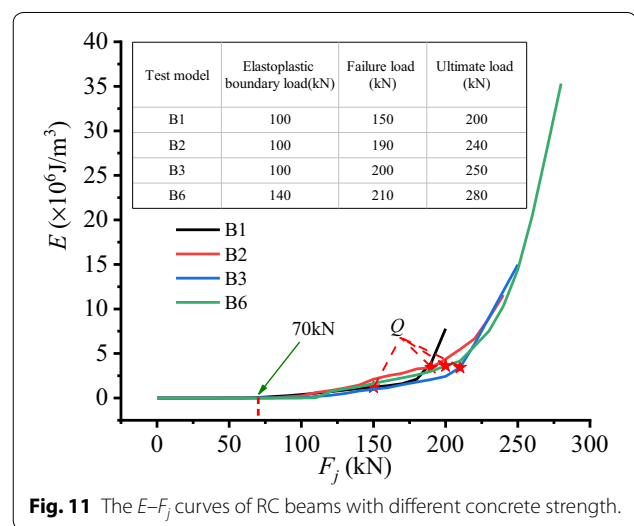


Therefore, the failure load 200 kN was a boundary for the RC beam, implying that the RC beam is in a quite unstable stressing state with potential risk and not suitable for continued loading from then on. In addition, it is obvious that there is a local strain reduction area in the lower part of the RC beam cross section. Hence, it could be speculated that the local strain reduction area may be caused by the strengthening effect of CFRP. Hereafter, with the increase of load, the area of the local strain reduction area gradually shrinks and then disappears. Thus, the strain fields expanded by the NSF method could reveal the sectional changing characteristics under loading, such as the detection of location strain concentration, etc., which can help researchers deeply understand the working behavior of the RC beam.

5 Investigation into RC Beams with Different Concrete Strength

5.1 The $E-F_j$ Curves of RC Beams with Different Concrete Strength

From the perspective of GSED, this paper investigates the effects of different concrete strength on the performance of RC beams strengthened by CFRP, the $E-F_j$ curves of these four specimens (B1, B2, B3 and B6) are plotted in the same graph, as shown in Fig. 11. A comparative analysis of the four results reveals that there is almost no difference among all the $E-F_j$ curves before 70



kN, indicating the strengthening performance of CFRP is not sufficiently exerted and the behavior of tested concrete beam strengthened with CFRP has few differences with the contrast concrete beam without wrapping CFRP. Subsequently, after 70 kN, the $E-F_j$ curves of these four specimens appears bifurcation, demonstrating the strengthening effect of CFRP become obvious due to the development of concrete cracks and the yield of

steel bars with load increase. In addition, the failure loads of B1, B2, B3 and B6 are determined by following the same method as proposed in Sect. 3, as listed in Fig. 11. Generally, these results indicate that the failure loads of RC beam strengthened with CFRP (B2, B3 and B6) are apparently enhanced than that of B1. Through comparing failure load and ultimate bearing capacity of the three different concrete strength, some research results can be concluded as follows:

1. As can be seen from the $E-F_j$ curves of RC beam strengthened with CFRP (B2, B3 and B6) in Fig. 11, the GSED values increase sharply after the failure load, which can be attributed to the rapid development of plastic deformation. Furthermore, the failure load can be considered as the characteristic load of the reinforcement effect. That is, although the RC beams can still bear load after the failure load, the CFRP is unable to provide enough reinforcement effect for the RC beams to maintain a stable stressing state.
2. The elasto-plastic boundary load of B1 is the same as that of B2 and B3, but the elasto-plastic boundary load of B6 is much larger, manifesting that the RC beam with higher concrete strength has longer elastic stage. The failure load of RC beams strengthened with CFRP (B2, B3 and B6) are significantly higher than that of the contrast RC beam (B1) and the failure load increases uniformly with the increasing concrete strength. In addition, the variation law of the ultimate load for B1, B2 and B3 is the same as the failure load but the ultimate load of B6 is significantly higher than that of B3. Moreover, the difference between ultimate load and failure load of B6 is 70 kN, while that of other specimens is 50 kN. In summary, the B6 compared with the remaining RC beams not only has the largest elasto-plastic boundary load, failure load and ultimate load, but also has the best bearing capacity after failure load. That is, CFRP can play a better role in strengthening performance of high strength concrete.

5.2 Investigation into the Stressing State Modes of RC Beams with Different Concrete Strength

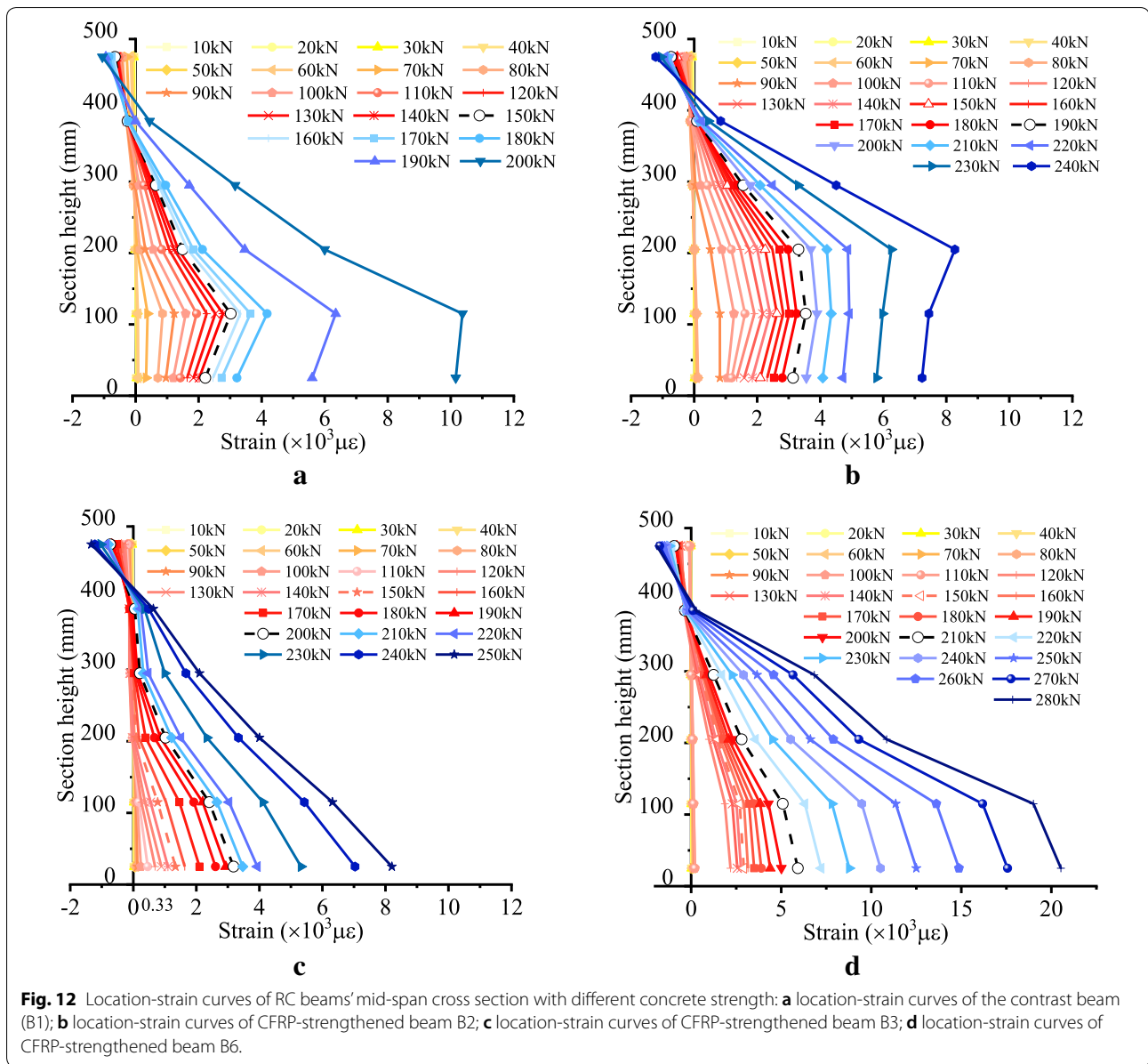
As shown in Fig. 12, the dash line corresponds to the failure load of the RC beams. It can be seen that the strain modes of concrete vividly show the stressing state characteristics of the RC beams strengthened by CFRP with different concrete strength. Through comparing these four graphs, several apparent conclusions can be summarized. Firstly, after the failure load (dash lines), the strains of these four RC beams present a sharp increase trend.

Hence, the strain modes of concrete also well reflect the mutation characteristics at failure load. Secondly, the strain growth rate of the contrast beam (B1) after failure load increases rapidly with the continuous expansion of concrete cracks and the yield of steel bars. However, after the failure load, the strain growth of these tested beams (B2, B3 and B6) is relatively uniform and the strain growth rate is relatively stable. Furthermore, through comparing B2, B3 and B6, it is apparent from Fig. 12a–c that the strain growth of B6 is the most uniform, and it still has good performance after the failure load. Therefore, the comparison of these four beams reveals that CFRP can manifest superior reinforcement performance in beams with high concrete strength.

Meanwhile, in order to investigate the strain characteristics of two layers of steel and CFRP, the strain-based stressing state modes are plotted, as shown in Fig. 13. These strengthened beams (B2, B3 and B6) show that the strain growth of the two layers of reinforcement and CFRP before the failure load increases slowly, but the strain of all three increases sharply after the failure load. In addition, it is obvious that the strain of CFRP of three beams is much smaller than that of two-layer steel bars in the early stress state, but the strain of CFRP gradually increases significantly with the increase of load. More specifically, in the early stress stage of the strengthened beam, the strain value of CFRP is very small due to its large elastic modulus. However, as the main stress part, the strain value of CFRP increases rapidly due to the development of concrete cracks and the yield of steel bars with load increases. Besides, it is apparent that the strain values of B3 and B6 are larger than that of the reinforcement, but the strain values of B2 beam are smaller than that of the reinforcement. That is, CFRP couldn't fully exert its superior reinforcement properties on low strength concrete beams.

5.3 Stress Fields of the RC Beams with Different Concrete Strength

Here, in order to reveal the sectional variation characteristics of the RC beams with different concrete strength, their strain fields around the characteristic load Q are plotted in Fig. 14. It can be seen that the lower sections of RC beams strengthened with CFRP (B2, B3, B6) all have local strain reduction regions, manifesting that the strengthening effect of CFRP restricts the strain development of the RC beam's lower part. Moreover, with the increase of load, the local strain reduction region will gradually shrink and then disappear, implying that the strengthening effect gradually disappears due to the stripping of CFRP from the concrete. Through comparing B2, B3 and B6, the local strain reduction region's area of RC beams strengthened with CFRP under failure load

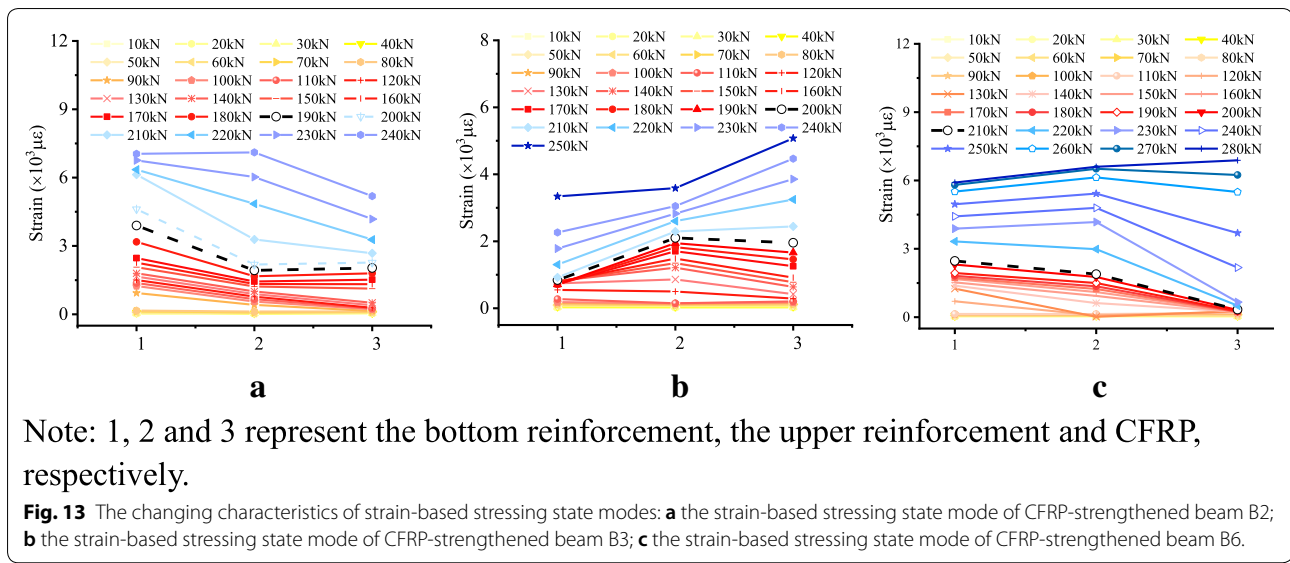


increases with the increase of concrete strength, which could be implied that high strength concrete with high elastic modulus can give full play to the strengthening effect of CFRP. From the perspective of the strain concentration area, the development degrees of strains are investigated, and it is found that the strain concentration area of the contrast RC beam (B1) without CFRP developed rapidly inward, while that of RC beams strengthened with CFRP (B2, B3, B6) gradually and slowly expanded upward along the side. That is to say, the strengthening effect of CFRP can also restrain the expansion of the strain concentration area. Therefore, the CFRP strengthening effect

of high strength RC beam (B6) is better than that of low strength RC beams (B2, B3).

5.4 Internal Forces of the RC Beams with Different Concrete Strength

After applying the NSF method to construct the strain fields, the sectional internal forces can also be obtained to further investigate the damage characteristics of the RC beams with different concrete strength. Equations (11) and (12) are proposed to calculate sectional internal forces of axial force (N) and bending moment (M_j), respectively:



$$N_j = \int_A \sigma dA = \sum_A \sigma_{ij} A_i \tag{12}$$

$$M_j = \int_A \sigma y dA = \sum_A \sigma_{ij} y_i A_i \tag{13}$$

where N_j is the axial force at j th load step, σ_{ij} is the longitudinal stress of the i th element at j -th load step, A_i is the area of the i th element, M_j is the bending moment at j th load step, y_i is vertical distances of the i -th element from the neutral axis.

It can be seen in Fig. 15a, b that the bending moment and axial force of the contrast beam (B1) are much smaller than that of the CFRP-strengthened beam under the whole loading process. That is to say, CFRP can effectively improve the bearing capacity of RC beams. In addition, compared with other CFRP-strengthened beams (B2 and B3), B6 beam can still bear large bending moment and axial force after the failure load Q , which also indicates that high-strength concrete can give full play to the strengthening performance of CFRP. Hence, in the design of CFRP reinforcement and maintenance, it is necessary to fully consider that the effect of concrete strength on the performance of CFRP reinforcement.

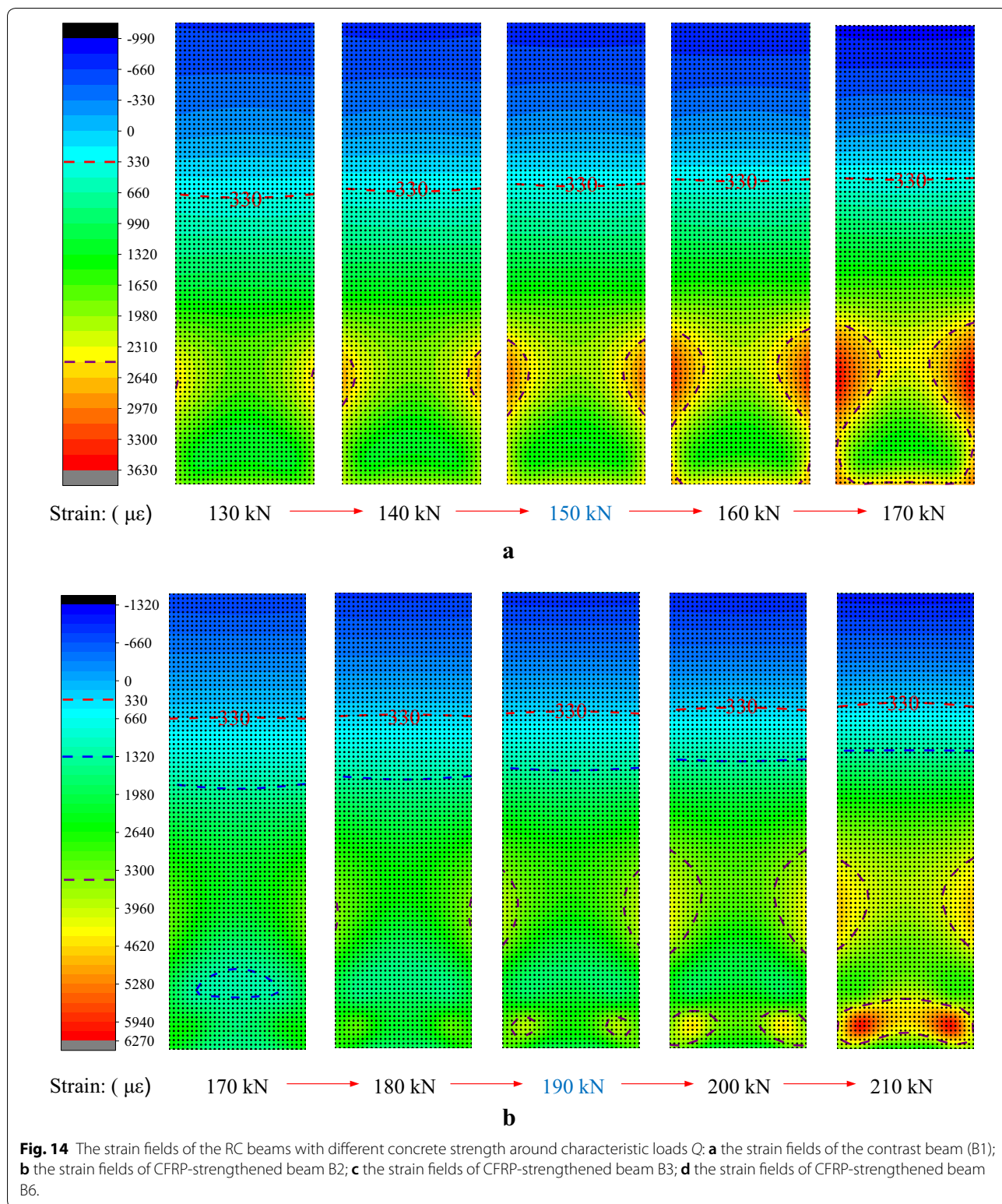
6 Investigation into RC Beams with Different Reinforcement Ratio

6.1 The $E-F_j$ Curves of Beams with Different Reinforcement Ratio

As shown in Fig. 16, the $E-F_j$ curves of these three specimens (B3, B4 and B5) with the same concrete strength and different reinforcement ratio are plotted in the

same graph, so as to investigate the effects of different reinforcement ratio on the performance of RC beams strengthened by CFRP. It is apparent that there is basically no difference between the four $E-F_j$ curves before 90 kN, manifesting that the reinforcement effect of CFRP is not sufficiently exerted and the behavior of the contrast RC beam without wrapping CFRP has few differences with tested RC beam strengthened with CFRP. Then, after 90 kN, the bifurcation of $E-F_j$ curves become obvious with load increase, signifying CFRP gradually begins to be effective owing to the development of concrete cracks and the yield of local steel bars. Additionally, the failure loads of B1, B3, B4 and B5 are also determined through following the same path as proposed in Section, as listed in Fig. 16. Overall, it is apparent from these results that the failure loads of concrete beam strengthened with CFRP (B3, B4 and B5) are significantly higher than that of B1. Through comparative analysis of failure load and ultimate bearing capacity of the four specimens, some research results can be concluded as follows:

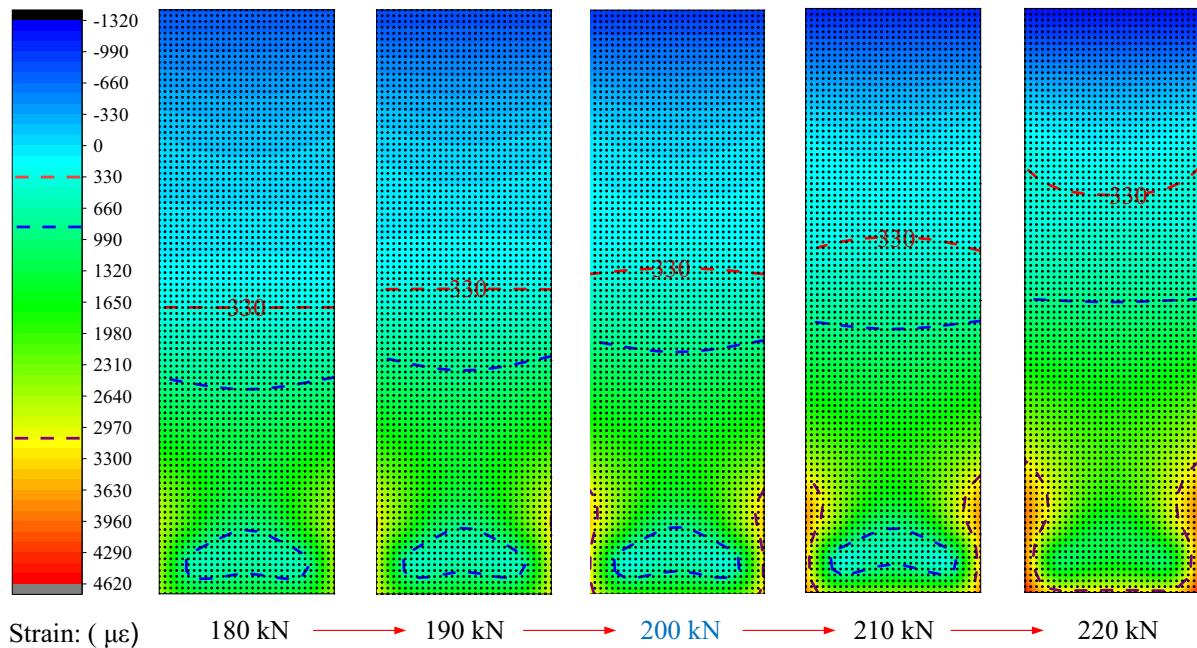
1. From the $E-F_j$ curves of RC beam strengthened with CFRP (B3, B4) in Fig. 16, it can be seen that the GSED value increases sharply after the failure load, which may be caused by the rapid development of plastic deformation. More specifically, the failure load can also be regarded as the characteristic load of the reinforcement effect. In other words, although the RC beams (B3, B4) can still bear a certain load after the failure load, the CFRP cannot provide enough reinforcement to keep the RC beams in a stable stressing state. In addition, it can be seen from Fig. 16 that the $E-F_j$ curve of B5 RC beam is still in



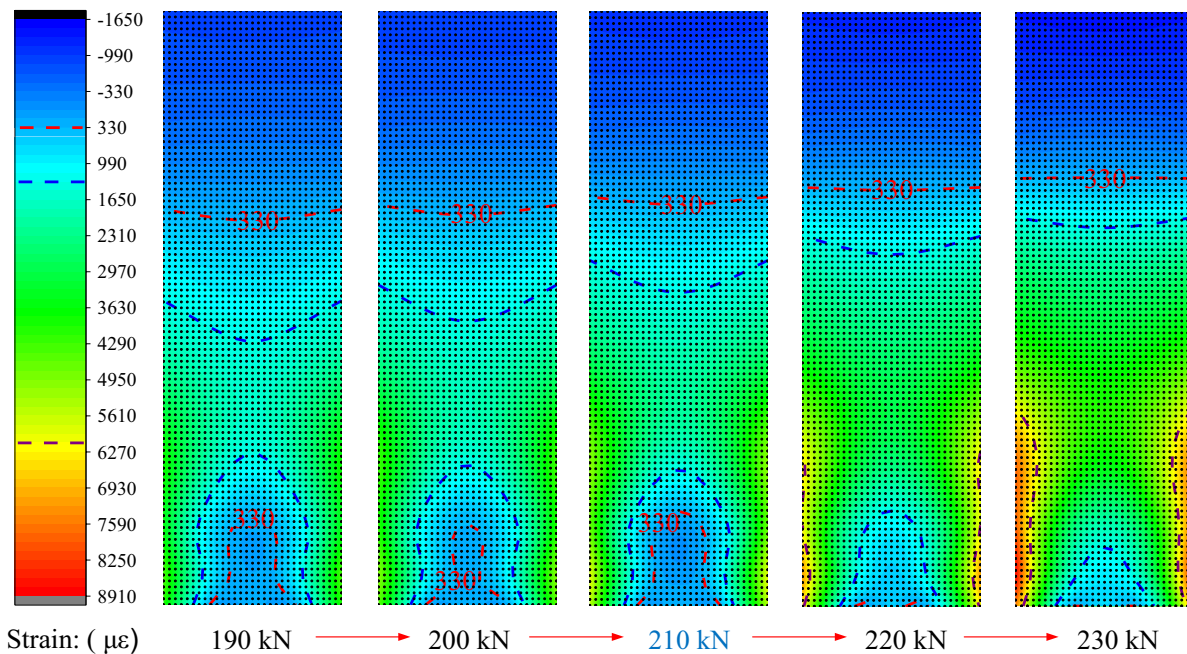
a relatively stable growth state after the failure load. Then the brittle failure of the B5 RC beam occurred suddenly, which could be implied that the concrete

in the compression area was crushed suddenly due to over-reinforcement.

2. By comparison, the failure load and ultimate load of RC beams strengthened with CFRP (B3, B4 and B5)



c



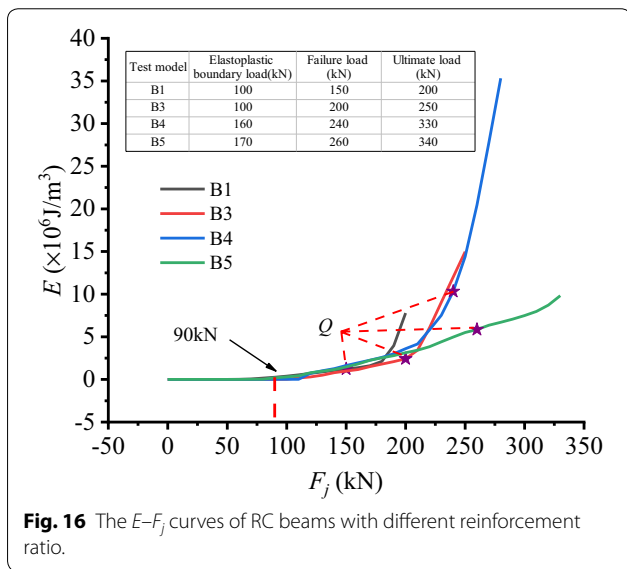
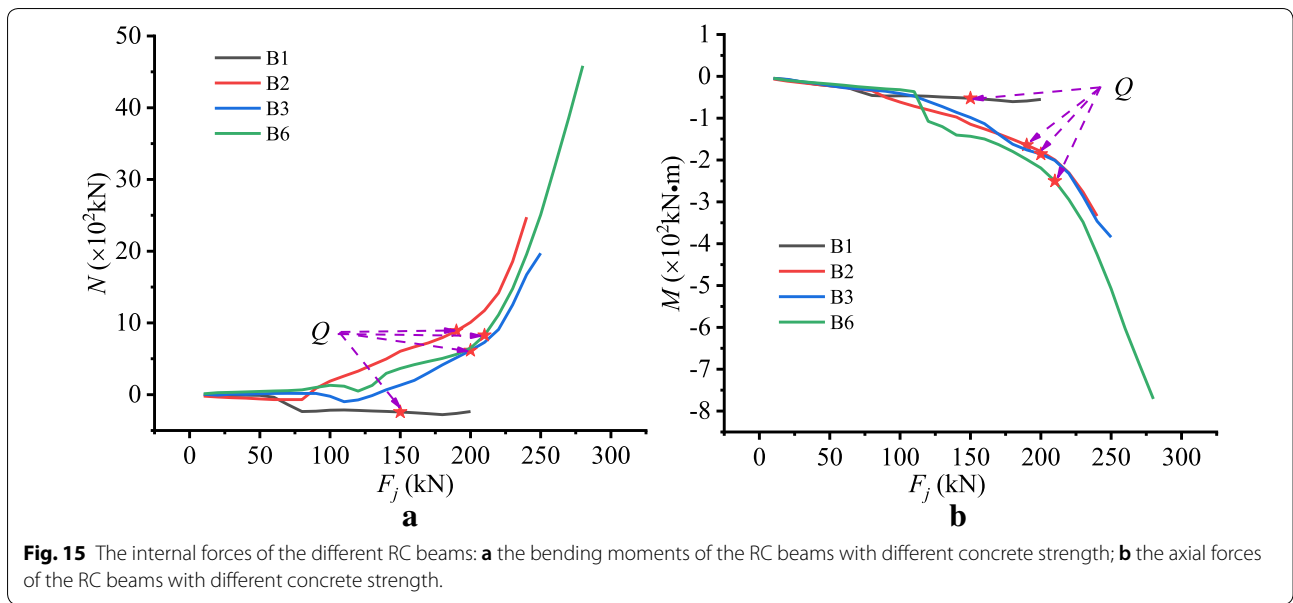
d

Fig. 14 continued

are significantly higher than that of the contrast RC beam (B1) and the failure load increases uniformly as the reinforcement ratio increases. However, with the reinforcement ratio increases, the increase of failure load and ultimate load is less and less.

6.2 Investigation into the Stressing State Modes of RC Beams with Different Reinforcement Ratio

As shown in Fig. 17, the dashed line represents the characteristic loads Q of the RC beams. Obviously, the strain modes of concrete can vividly reveal the stressing state



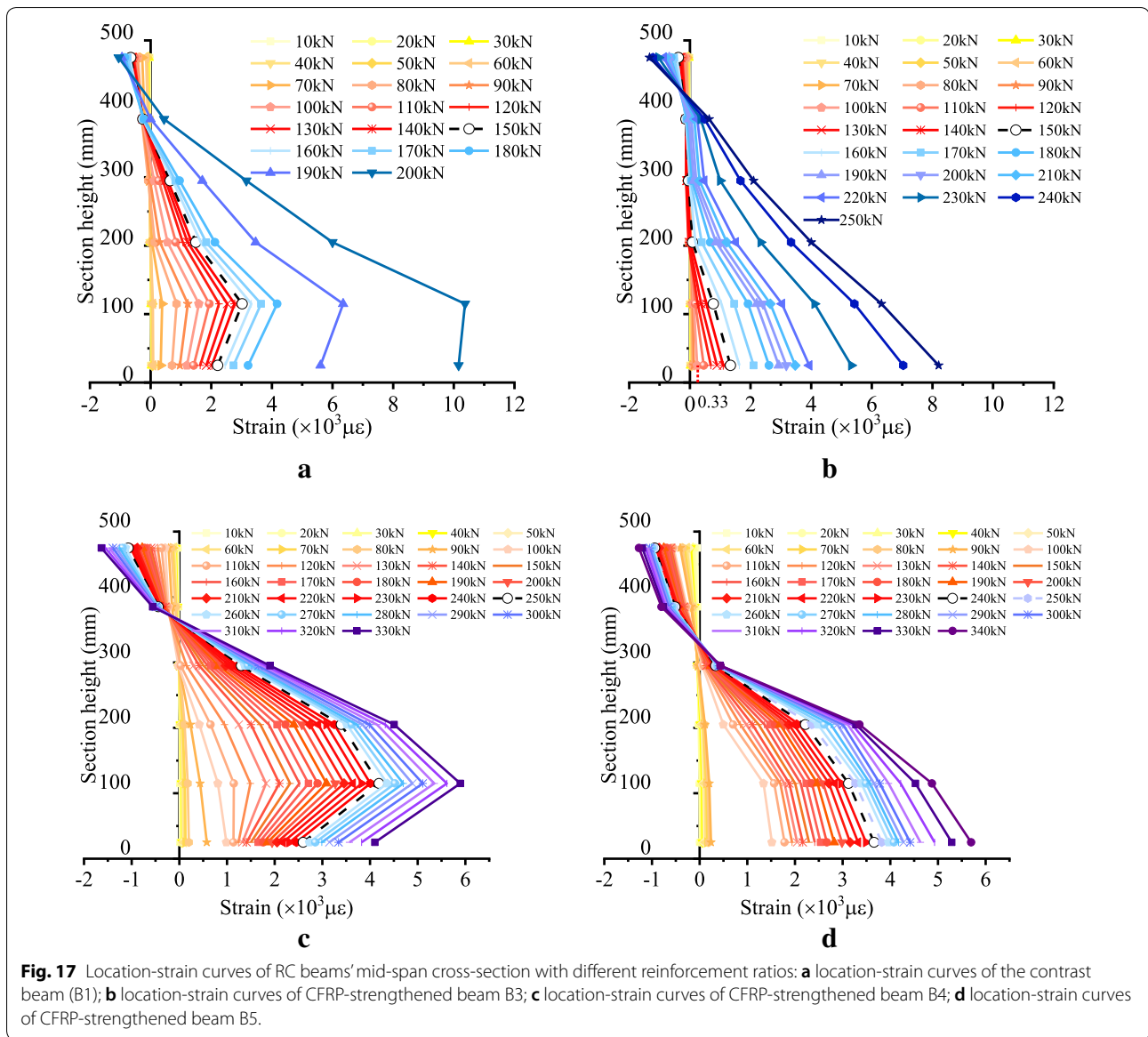
characteristics of the RC beams strengthened by CFRP with different reinforcement ratio. Hence, several apparent conclusions can be obtained by comparing these four graphs. After the failure load (dash lines), the strains of B1 and B3 RC beams present a sharp increase trend whether the over-reinforcement beams (B4, B5) are strengthened by CFRP or not. As shown in Sect. 4, the strain growth rates of B1 and B3 have been analyzed in detail. After the failure load, the strain growth of these tested beams (B3, B4 and B5) is relatively uniform and the strain growth rate is relatively stable. In addition, the strengthening effect of CFRP is more obvious in the

over-reinforcement beams (B4, B5) than in balanced-reinforced beam (B3). More specifically, through comparing B4 and B5, it can be seen that the strengthening effect of these two beams is basically similar, signifying that the brittle failure occurs to the upper concrete of the RC beams due to over reinforcement. Therefore, reasonable reinforcement is very necessary to make full use of the reinforcement performance of CFRP.

As shown in Fig. 18, the strain-based stressing state modes are plotted to investigate the strain characteristics of two layers of steel and CFRP. As for the strain-based stressing state modes of the over-reinforcement beams (B4, B5), before and after the failure load Q , the strain growth of the upper reinforcement, bottom reinforcement and CFRP still increases uniformly. Here, the change characteristics of the strain-based stressing state modes are similar to those shown in Fig. 17. Hence, all the different forms of strain modes can reflect a similar change pattern of RC beams with different reinforcement ratios vividly.

6.3 Stress Fields of the RC Beams with Different REINFORCEMENT Ratio

To investigate the common sectional damage characteristics of the RC beams with different reinforcement ratio, their strain fields around their respective characteristic load Q are plotted in Fig. 19. The variation of B1 and B3 beams before and after the failure load has been described in Sect. 4. Through comparing B3, B4 and B5, it can be found that the crack area of balanced-reinforced beam (B3) expands upward with the increase

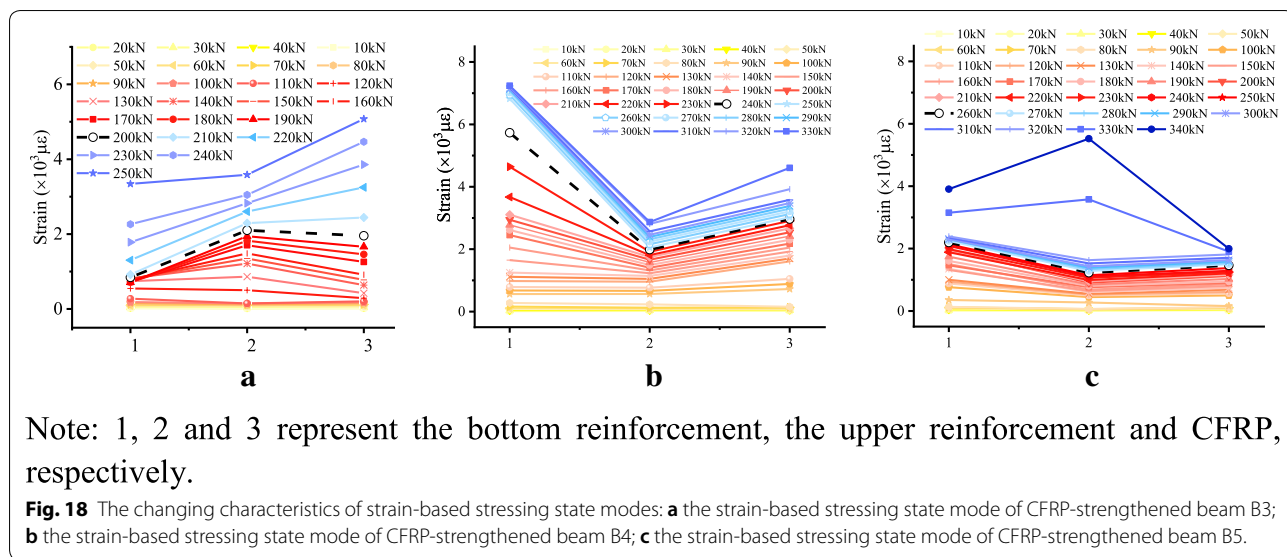


of load, while the cracked area of over-reinforcement beams (B4, B5) and contrast RC beam (B1) is basically unchanged, which indicating that the compression zone height of B1, B4 and B5 beams reaches the limit height and the strengthening effect of CFRP of B4 and B5 beams begin to take effect before and after the failure load. From the perspective of the strain concentration area, it can be seen that The strain fields development of B4 and B5 beams are different from B3, that is, the excessive reinforcement of B4 and B5 beams causes the strengthening of CFRP to take effect before and after the failure load. Therefore, it is necessary to

allocate reasonable reinforcement to give full play to the strengthening effect of CFRP.

6.4 Internal forces of the RC beams with different reinforcement ratio

As mentioned above, based on the NSF method, the internal bending moment and axial force could be obtained to further investigate the damage characteristics of the RC beams with different reinforcement ratio. It is apparent from Fig. 20 that CFRP can efficaciously improve the bearing capacity of RC beams with different reinforcement ratio. More specifically, compared to the contrast beam, the CFRP-strengthened beams (B3,



B4 and B5) still have a larger plastic development after the failure load Q . Additionally, the maximum axial force and bending moment appear on the balanced-reinforced beam (B3), reflecting that too much reinforcement has no obvious effect on the strengthening performance of CFRP. Therefore, it is very important to allocate reasonable steel bars in CFRP reinforcement and reconstruction.

7 Conclusions

An experimental investigation is carried out on one unreinforced RC beam and five CFRP-strengthened RC beams with different concrete strength and reinforcement ratio. With the application of structural stressing state theory and methodology, the changing characteristics and unseen knowledge of tested RC beams are revealed. The M–K criterion is adopted to detect the qualitative leap characteristics and the stressing state of the beam is divided into three stages, respectively elastic, elastic–plastic and failure stage. The characteristic load Q is defined as the updated failure load, implying the beginning of the beam’s failure process. And the effectiveness and rationality of the M–K criterion are verified through analyzing the changing trends and distribution patterns of stressing state modes.

Due to the limited strain data, which could not reflect the whole structure’s working behavior clearly, the NSF method with clear physical meanings is proposed to reasonably interpolate the strains at unsampled locations. The obtained strain fields and internal forces of cross-sections can describe the stressing state of RC beam accurately and reflect the qualitative leap characteristics at failure load vividly.

By comparison of the RC beams with different concrete strength, these results indicate that CFRP-strengthened RC beams with high concrete strength can better exert the strengthening properties of CFRP. In addition, comparing the results of the RC beams with different reinforcement ratios, it can be seen that balanced-reinforced beams strengthened by CFRP have a better reinforcement effect.

Applying the stressing state theory to the measured experimental data, the achieved results reveal stressing state characteristics of RC beams and accurately predict the failure load for RC beams. Furthermore, the analysis of the RC beams’ stressing state explores a new way to the working behavior and the unseen knowledge could provide an appropriate reference for structural design and practice of CFRP reinforcement and maintenance, which could considerably promote the benefits in saving material, structural safety, and structural working rationality.

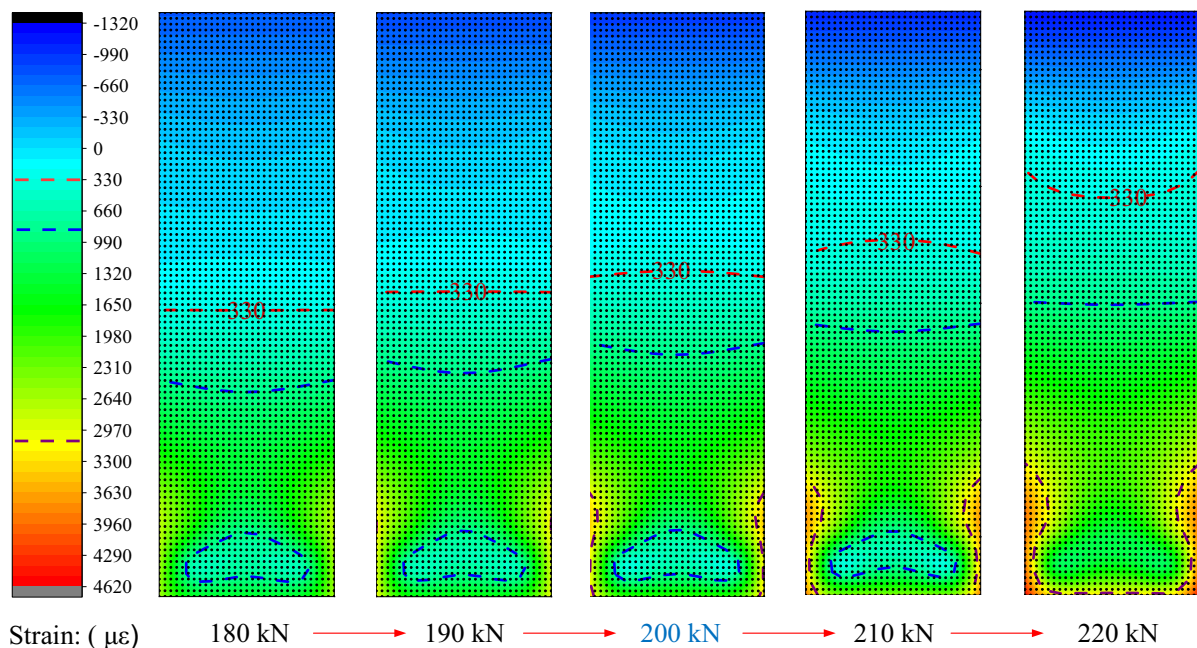
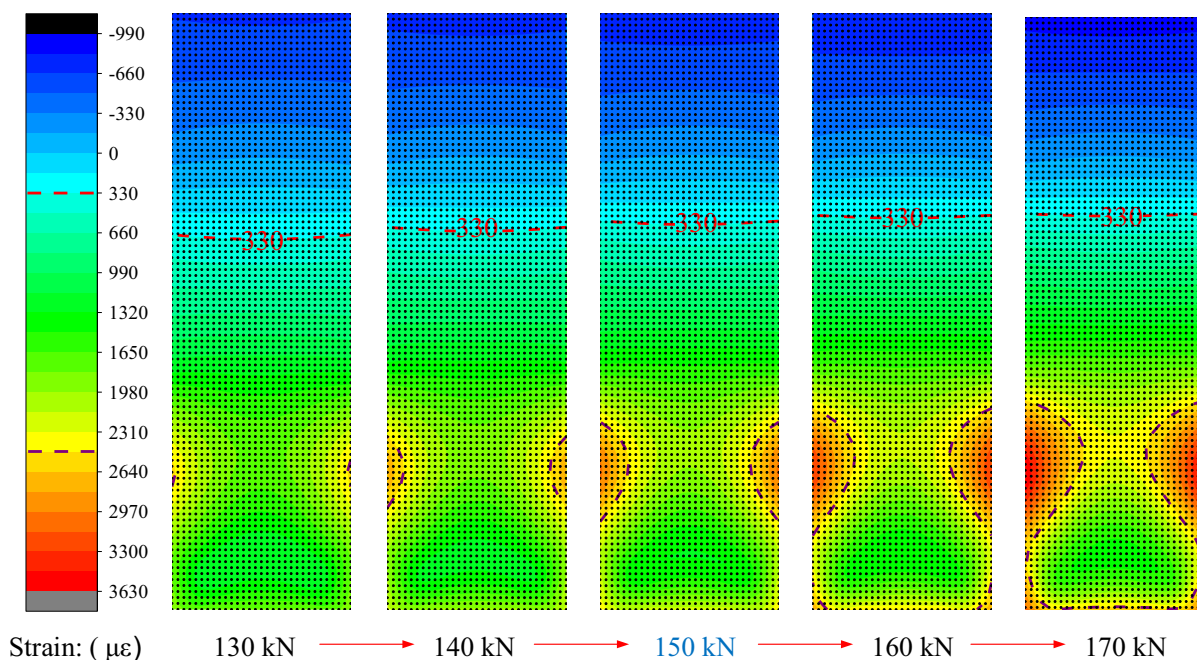
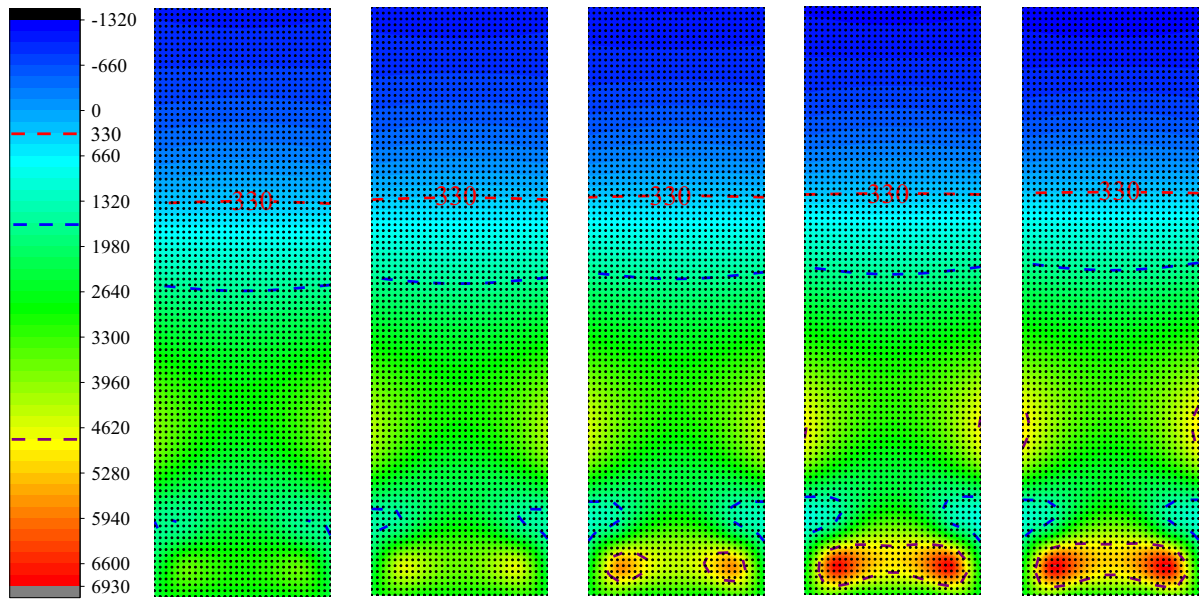
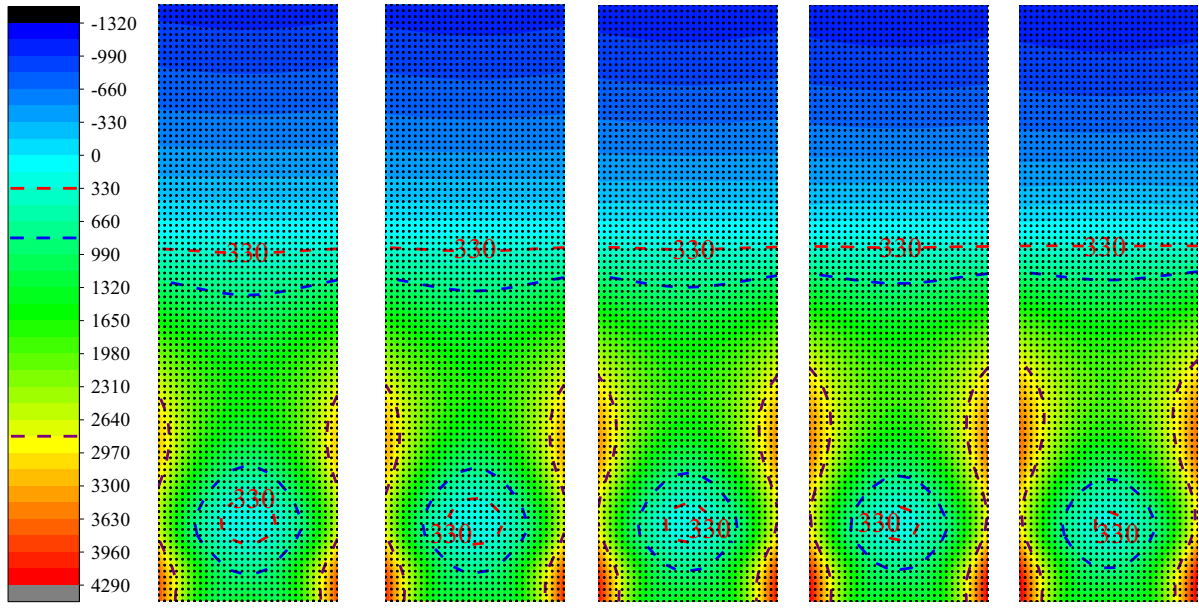


Fig. 19 The strain fields of the RC beams with different reinforcement ratio around characteristic loads Q : **a** the strain fields of the contrast beam (B1); **b** the strain fields of CFRP-strengthened beam B3; **c** the strain fields of CFRP-strengthened beam B4; **d** the strain fields of CFRP-strengthened beam B5.



Strain: ($\mu\epsilon$) 220 kN → 230 kN → 240 kN → 250 kN → 260 kN

c



Strain: ($\mu\epsilon$) 240 kN → 250 kN → 260 kN → 270 kN → 280 kN

d

Fig. 19 continued

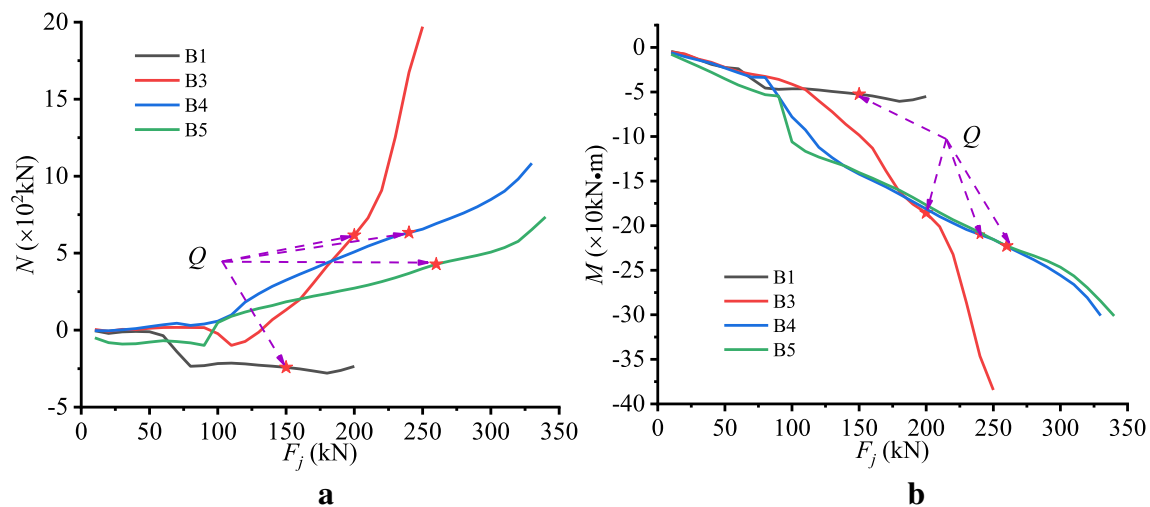


Fig. 20 The internal forces of the different RC beams: **a** the bending moments of the RC beams with different reinforcement ratio; **b** the axial forces of the RC beams with different reinforcement ratio.

Acknowledgements

The authors would like to express their gratitude to Yajun He for carrying out the excellent RC beams experiment and giving the experimental data in detail in his dissertation thesis. The authors would also like to thank the members of the HIT 504 office for their selfless help and useful suggestions.

Authors' contributions

JH and SJ were responsible for data collection, analysis and interpretation. HX, JS and BY helped perform the analysis with constructive discussions. JH wrote the first draft of the article. All authors read and approved the final manuscript.

Author information

Jun Shi, Associate Professor, School of Civil Engineering, Central South University, Changsha 410075, China.

Jie Huang, PhD Student, School of Civil Engineering, Harbin Institute of Technology, Harbin 150090, China.

Hengheng Xiao, PhD Student, School of Civil Engineering, Harbin Institute of Technology, Harbin 150090, China.

Jiyang Shen, PhD Student, School of Civil Engineering, Harbin Institute of Technology, Harbin 150090, China.

Baisong Yang, PhD Student, School of Civil Engineering, Harbin Institute of Technology, Harbin 150090, China.

Funding

None.

Availability of data and materials

The datasets used and analysed during the current study are available from the corresponding author on reasonable request.

Competing interests

The authors declare that they have no competing interests.

Author details

¹ School of Civil Engineering, Central South University, Changsha, China.

² National Engineering Laboratory for High Speed Railway Construction, Changsha, China. ³ Key Lab of Structures Dynamic Behavior and Control of the Ministry of Education, Harbin Institute of Technology, Harbin 150090, China.

Received: 20 February 2020 Accepted: 5 May 2020

Published online: 14 September 2020

References

- Abualnour, M., Chikh, A., Hebali, H., Kaci, A., Tounsi, A., Bousahla, A. A., et al. (2019). Thermomechanical analysis of antisymmetric laminated reinforced composite plates using a new four variable trigonometric refined plate theory. *Computers and Concrete*, 24(6), 489–498.
- Ali, A., Abdalla, J., Hawileh, R., & Galal, K. (2014). CFRP mechanical anchorage for externally strengthened RC beams under flexure. *Physics Procedia*, 55, 10–16.
- Altin, S., et al. (2010). Improving shear capacity and ductility of shear-deficient RC beams using CFRP strips. *Journal of Reinforced Plastics and Composites*, 29(19), 2975–2991.
- Ashour, A. F., et al. (2004). Flexural strengthening of RC continuous beams using CFRP laminates. *Cement & Concrete Composites*, 26(7), 765–775.
- Attari, N., Amziane, S., & Chemrouk, M. (2012). Flexural strengthening of concrete beams using CFRP, GFRP and hybrid FRP sheets. *Construction and Building Materials*, 37, 746–757.
- Ayers, P. W. (2006). Information theory, the shape function, and the Hirshfeld atom. *Theoretical Chemistry Accounts*, 115(5), 370–378.
- Balamuralikrishnan, R., & Jeyasehar, C. A. (2009). Flexural behavior of RC beams strengthened with carbon fiber reinforced polymer (CFRP) fabrics. *The Open Civil Engineering Journal*, 3(1), 102–109.
- Belbachir, N., Draich, K., Bousahla, A. A., Bourada, M., Tounsi, A., & Mohammadimehr, M. (2019). Bending analysis of anti-symmetric cross-ply laminated plates under nonlinear thermal and mechanical loadings. *Steel and Composite Structures*, 33(1), 81–92.
- Benjeddou, O., Ouezdou, M. B., & Bedday, A. (2007). Damaged RC beams repaired by bonding of CFRP laminates. *Construction and Building Materials*, 21(6), 1301–1310.
- Bousahla, A. A., Bourada, F., Mahmoud, S. R., Tounsi, A., Algarni, A., Bedia, E. A., et al. (2020). Buckling and dynamic behavior of the simply supported CNT-RC beams using an integral-first shear deformation theory. *Computers and Concrete*, 25(2), 155.
- Dias, S. J. E., et al. (2018). Behavior of RC beams flexurally strengthened with NSM CFRP laminates. *Composite Structures*, 201, 363–376.
- Draiche, K., Bousahla, A. A., Tounsi, A., Alwabli, A. S., Tounsi, A., & Mahmoud, S. R. (2019). Static analysis of laminated reinforced composite plates using

- a simple first-order shear deformation theory. *Computers and Concrete*, 24(4), 369–378.
- Draoui, A., Zidour, M., Tounsi, A., & Adim, B. (2019). Static and dynamic behavior of nanotubes-reinforced sandwich plates using (FSDT). *Journal of Nano Research*, 57, 117–135.
- El-Ghandour, A. A. (2011). Experimental and analytical investigation of CFRP flexural and shear strengthening efficiencies of RC beams. *Construction and Building Materials*, 25(3), 1419–1429.
- Hawileh, R. A., Nawaz, W., Abdalla, J. A., & Saqan, E. I. (2015). Effect of flexural CFRP sheets on shear resistance of reinforced concrete beams. *Composite Structures*, 122, 468–476.
- Hawileh, R. A., Rasheed, H. A., Abdalla, J. A., & Al-Tamimi, A. K. (2014). Behavior of reinforced concrete beams strengthened with externally bonded hybrid fiber reinforced polymer systems. *Materials and Design*, 53, 972–982.
- Hirsch, R. M., Slack, J. R., & Smith, R. A. (1982). Techniques of trend analysis for monthly water quality data. *Water Resources Research*, 18(1), 107–121.
- Huang, Y., Zhang, Y., Zhang, M., & Zhou, G. (2014). Method for predicting the failure load of masonry wall panels based on generalized strain-energy density. *Journal of Engineering Mechanics*, 140(8), 04014061.
- Karami, B., Shahsavari, D., Janghorban, M., & Tounsi, A. (2019). Resonance behavior of functionally graded polymer composite nanoplates reinforced with graphene nanoplatelets. *International Journal of Mechanical Sciences*, 156, 94–105.
- Kendall, M. G. (1948). *Rank correlation methods*. Egypt: Griffin.
- Li, L. J., et al. (2006). An experimental and numerical study of the effect of thickness and length of CFRP on performance of repaired reinforced concrete beams. *Construction and Building Materials*, 20(10), 901–909.
- Mann, H. B. (1945). Nonparametric tests against trend. *Econometrica*, 13, 245–259.
- Medani, M., Benahmed, A., Zidour, M., Heireche, H., Tounsi, A., Bousahla, A. A., et al. (2019). Static and dynamic behavior of (FG-CNT) reinforced porous sandwich plate using energy principle. *Steel and Composite Structures*, 32(5), 595–610.
- Osman, B. H., et al. (2019). Effect of reinforcement ratios on shear behavior of concrete beams strengthened with CFRP sheets. *HBRC Journal*, 14(1), 29–36.
- Padhi, G. S., Shenoj, R. A., Moy, S. S. J., & McCarthy, M. A. (2001). Analytic integration of kernel shape function product integrals in the boundary element method. *Computers & Structures*, 79(14), 1325–1333.
- Rafi, M. M., Nadjai, A., Ali, F., & Talamona, D. (2008). Aspects of behaviour of CFRP reinforced concrete beams in bending. *Construction and Building Materials*, 22(3), 277–285.
- Sahla, M., Saidi, H., Draiche, K., Bousahla, A. A., Bourada, F., & Tounsi, A. (2019). Free vibration analysis of angle-ply laminated composite and soft core sandwich plates. *Steel and Composite Structures*, 33(5), 663.
- Salama, A. S. D., Hawileh, R. A., & Abdalla, J. A. (2019). Performance of externally strengthened RC beams with side-bonded CFRP sheets. *Composite Structures*, 212, 281–290.
- Shi, J., Li, W., Zheng, K., Yang, K., & Zhou, G. (2018). Experimental investigation into stressing state characteristics of large-curvature continuous steel box-girder bridge model. *Construction and Building Materials*, 178, 574–583.
- Spadea, G., Swamy, R. N., & Bencardino, F. (2001). Strength and ductility of RC beams repaired with bonded CFRP laminates. *Journal of Bridge Engineering*, 6(5), 349–355.
- Toutanji, H., Zhao, L., & Zhang, Y. (2006). Flexural behavior of reinforced concrete beams externally strengthened with CFRP sheets bonded with an inorganic matrix. *Engineering Structures*, 28(4), 557–566.
- He Y. J. 2016. The flexural capacity of reinforced concrete short beams strengthened with carbon fiber reinforced polymer sheets (CFRP). M.S. Thesis. Zhengzhou University (in Chinese).
- Zhou, G. C., Rafiq, M. Y., Bugmann, G., & Easterbrook, D. J. (2006). Cellular automata model for predicting the failure pattern of laterally loaded masonry wall panels. *Journal of Computing in Civil Engineering*, 20(6), 400–409.

Publisher's Note

Springer Nature remains neutral with regard to jurisdictional claims in published maps and institutional affiliations.

Submit your manuscript to a SpringerOpen® journal and benefit from:

- Convenient online submission
- Rigorous peer review
- Open access: articles freely available online
- High visibility within the field
- Retaining the copyright to your article

Submit your next manuscript at ► [springeropen.com](https://www.springeropen.com)
